Rewired NAD^+ metabolism promotes NF-κB-mediated oxidative stress and disrupts lipid homeostasis in liver fibrosis progression

Hiu-Lok Ngan,[1] Jacinth Wing-Sum Cheu,[2,3] Kenneth Kin-Leung Kwan,[2,3] Carmen Chak-Lui Wong,[2,3] Hong Yan,[1,4,] Zongwei Cai[1,5,]**

[1]State Key Laboratory of Environmental and Biological Analysis, Department of Chemistry, Hong Kong Baptist University, Hong Kong 999077 P. R. China

[2]State Key Laboratory of Liver Research, Department of Pathology, Li Ka Shing Faculty of Medicine, The University of Hong Kong, Hong Kong 999077 P. R. China

[3]Centre for Oncology and Immunology, Hong Kong Science Park, Hong Kong 999077 P. R. China

[4]Department of Biology, Hong Kong Baptist University, Hong Kong 999077 P. R. China

[5]Eastern Institute of Technology, Ningbo 315200 P. R. China

*Corresponding authors: Drs. Hong Yan and Zongwei Cai

E-mails: hongyan@hkbu.edu.hk; zwcai@hkbu.edu.hk

Keywords: hepatocellular carcinoma, nicotinamide, sirtuin 1, *de novo* lipogenesis, multi-omics

ABSTRACT

Chronic liver fibrosis significantly increases the risk of hepatocellular carcinoma (HCC), a leading cause of cancer-related deaths. However, the molecular mechanisms linking fibrosis to inflammation-associated HCC development remain unclear, complicating early diagnosis and intervention. In this study, we employ multi-omics analyses, including untargeted and targeted metabolomics, lipidomics, and transcriptomics, in a mouse model of chemically induced liver fibrosis and HCC, integrating publicly available transcriptome data from LX-2 human hepatic stellate cell (HSC) line. Our results reveal a profound rewiring of NAD^+ metabolism as a central driver of metabolic disturbance. Analysis of bulk liver tissue shows increased activity of the kynurenine pathway of tryptophan metabolism, enhancing NAD^+ precursor production. Hepatic nicotinamide (NAM) levels decrease due to elevated expression of NAM *N*-methyltransferase (*Nnmt*) in HSCs. Despite reduced hepatic NAM, serum NAD^+ level rise and is compartmentalized, triggering a disruption in NAD^+ homeostasis and activating NF-κB-

mediated oxidative stress pathways. Moreover, lipid dysregulation occurs, with NF-κB dominating the regulation of SIRT1/SREBP-controlled lipogenic and cholesterogenic genes, leading to imbalances in hepatic and serum lipids. These insights elucidate connections between NAD^+ metabolism, inflammation, and lipid dysregulation, potentially aiding in developing diagnostic biomarkers and therapeutic targets for non-viral HCC.

Key Points

1. The integration of untargeted and targeted metabolomics identifies the metabolic pathways that are associated with the development of hepatocellular carcinoma (HCC) and the potential role of disturbances in NAD^+ metabolism as a central driver of metabolic dysregulation in hepatic fibrosis, validated across transcriptomics.
2. Fibrosis-associated HCC is linked to the depletion of nicotinamide and a cascade of metabolic disturbances that promote inflammation and oxidative stress in hepatic stellate cells.
3. Targeted analysis of the metabolites in the discriminative pathways along a continuum of fibrosis-cirrhosis-HCC discovers several potential tissue and serum biomarkers for monitoring disease progression.
4. Multi-omics analysis (i.e., metabolomics, lipidomics, and transcriptomics) reveals complex interplay between NAD^+ metabolism, NF-κB-mediated oxidative stress, and lipid homeostasis in fibrosis-associated HCC development.

Abbreviations

3-HAA	3-Hydroxyanthranilate
AAG	Alanine/aspartate/glutamate
Acat2	Acyl-CoA:cholesterol acyltransferase 2
Acly	ATP citrate lyase
AMC	Age-matched control
Aox1	Aldehyde oxidase 1
BA	Bile acid
CCl4	Carbon tetrachloride
Cpt1a	Carnitine palmitoyltransferase 1A
DEG	Differentially expressed gene
DEN	Diethylnitrosamine

DG	Diglyceride
DNL	*De novo* lipogenesis
ESI	Electrospray ionization
FA	Fatty acid
FAO	Fatty acid oxidation
Fasn	Fatty acid synthase
Haao	3-Hydroxyanthranilate 3,4-dioxygenase
HBV	Hepatitis B virus
HCC	Hepatocellular carcinoma
Hmgcr	3-Hydroxy-3-methylglutaryl-CoA reductase
Hmgcs1	3-Hydroxy-3-methylglutaryl-CoA synthase 1
HSC	Hepatic stellate cell
IFN-γ	Interferon gamma
m/z	Mass-to-charge ratio
MS	Mass spectrometry
NA	Nicotinic acid
NAD^+	Nicotinamide adenine dinucleotide
NAFLD	Non-alcoholic fatty liver disease
NAM	Nicotinamide
Nampt	Nicotinamide phosphoribosyltransferase
NASH	Non-alcoholic steatohepatitis
Nfkb1	Nuclear factor kappa B subunit 1
Nmnat1	Nicotinamide mononucleotide adenylyltransferase 1
Nnmt	Nicotinamide N-methyltransferase
Prkag2	5'-AMP-activated protein kinase subunit gamma-2
QC	Quality control
Qprt	Quinolinate phosphoribosyl transferase
RNA-Seq	RNA sequencing
RPLC	Reverse-phase liquid chromatography
Sirt	Sirtuin
Srebf1	Sterol regulatory element-binding protein 1
Srebf2	Sterol regulatory element-binding protein 2
SREBP	Sterol regulatory element-binding protein
Tdo2	Tryptophan 2,3-dioxygenase

TG	Triglyceride
TGF-β1	Transforming growth factor beta 1

1. Introduction

Cancer represents a significant global health burden, according for nearly 10 million deaths worldwide in 2020 [1]. Among the various cancer types, liver cancer stands out as a particularly devastating chronic disease and is the emerging one in the United States [2]. While ranking 7th in incidence, it was the 3rd leading cause of cancer-related mortality [3], with a strikingly high mortality-to-incidence ratio of nearly 1:1 [3]. This underscores the lethality of liver cancer compared to other malignancies.

Early detection and intervention are critical for improving patient outcomes, yet liver cancer is often diagnosed at advanced stages, less treatable stages [4]. Hepatocellular carcinoma (HCC) is the most common subtype of liver cancer [5]. Its risk factors mostly are related to cirrhosis [6], that can be induced by hepatitis B virus (HBV) and hepatitis C virus, alcohol, and metabolism-associated factors, such as diabetes, obesity, non-alcoholic fatty liver disease (NAFLD) [7]. Chronic liver injury triggers a sustained wound-healing response characterized by the activation and differentiation of hepatic stellate cells (HSCs) into collagen-producing myofibroblasts, leading to the progressive scarring of the liver known as fibrosis [8]. Advanced liver fibrosis results in cirrhosis and involves in hepatocarcinogenesis [9]. Hence, elucidating the fibrosis-dependent mechanisms driving tumor progression will be crucial to rationalizing the development of antifibrotic therapies as an early intervention strategy.

The current body of clinical research of inflammation-associated HCC has primarily focused on analyzing serum samples from patients diagnosed with HCC [10–13], cirrhosis [13,14], fibrosis [15], or HBV infection [10,13]. Serum metabolomics is advantageous for the discovery of diagnostic biomarkers due to its relatively non-invasive sampling approach. However, in the context of early detection and disease intervention, tissue samples are necessary to examine the underlying molecular underpinnings driving the transition from chronic liver disease. Unfortunately, the availability of clinical tissue samples is often limited to the advanced stage of disease at the time of diagnosis. While there are several studies on HCC [10,13,16,17] and cirrhosis [18], tissue samples from the fibrotic stage are scarce [19]. This limitation in access to well-characterized fibrotic tissue samples represents a significant challenge that hinders our understanding of the fibrosis-dependent tumorigenic mechanisms. To fill this knowledge gap, animal models of liver fibrosis and inflammation-associated HCC are needed for a

87 comprehensive investigation of the metabolic, signaling, and regulatory alterations in rodent
88 liver tissue prior to clinical investigation [20,21].
89 In this study, we employ a diethylnitrosamine-carbon tetrachloride (DEN-CCl_4) chemical-
90 induced male mouse model to monitor the etiology and progression of fibrosis-associated HCC
91 by multi-omics analyses, including inter-validation between metabolomics, lipidomics, and
92 transcriptomics and external validation by a transcriptome set of activated human HSCs. We
93 characterize metabolic disturbances in tryptophan metabolism, nicotinate/nicotinamide
94 metabolism, fatty acid (FA) metabolism, alanine/aspartate/glutamate (AAG) metabolism, and
95 citrate cycle throughout the progression stages (fibrosis, cirrhosis, and HCC) and identify
96 several potential diagnostic serum and tissue biomarkers for disease monitoring. We confirm
97 the dysregulated metabolic pathways discovered through our multi-omics analyses using RNA
98 sequencing (RNA-Seq) and assess their occurrence and regulation within HSCs. Overall, our
99 results demonstrate NAM depletion by the upregulation of NAM *N*-methyltransferase (*Nnmt*)
100 in HSCs derives the rewiring of nicotinamide adenine dinucleotide (NAD^+) metabolism.
101 Disturbances in NAD^+ homeostasis and its associated pathways trigger inflammation and lipid
102 dysregulation, that create a pro-tumorigenic microenvironment in the fibrotic liver. These
103 findings may ultimately contribute to improved early detection and more effective interventions
104 to prevent the devastating progression from chronic liver disease to HCC.
105

106 **2. Materials and Methods**

107 **2.1. Chemical and Reagents**

108 Absolute Ethanol (EtOH), chloroform, formic acid (99–100%), LC/MS-grade acetonitrile
109 (ACN), methanol (MeOH), and isopropanol (IPA) were obtained from VWR Chemicals BDH®
110 (Poole, UK). 2-Oxo-glutaric acid, 4-aminobutanoic acid, 5-hydroxy-L-tryptophan, (S)-malic
111 acid, chenodeoxycholic acid, cis-aconitic acid, citric acid, fumaric acid, glycocholate, indole,
112 indoleacetic acid, isocitric acid, L-alanine, L-asparagine, L-aspartic acid, L-glutamic acid, L-
113 glutamine, L-kynurenine, melatonin, nicotinamide (NAM), NAM adenine dinucleotide (NAD^+),
114 $NADP^+$, NADPH, nicotinic acid, oxaloacetic acid, serine, serotonin, succinic acid, taurine,
115 taurochenodeoxycholic acid, taurocholic acid, tryptophan, and quinolinic acid were obtained
116 from Sigma-Aldrich (St. Louis, MO, USA). 2-Amino-4-(2-amino-3-hydroxy-phenyl)-4-oxo-
117 butanic acid, 2-amino-4-(2-formamidophenyl)-4-oxo-butanoic acid, 5-hydroxy-indoleacetate,
118 5-methoxyindole-3-acetic acid, cholic acid, indole-3-acetaldehyde, maleic acid, pyridoxal, and
119 taurochenodeoxycholic acid were purchased from Yuanye (Guangzhou, CN). 3-

120 Hydroxyanthranilc acid, 4-pyridoxic acid, (Z)-4-amino-4-oxobut-2-enoic acid,
121 glycochenodeoxycholic acid, indole-3-pyruvic acid, *N*-acetyl-5-hydroxytryptamine, nicotinuric
122 acid, oxoadipic acid, and pyridoxine were collected from TargetMol (Boston, MA, USA). 5-
123 Methoxytryptamine, 6-hydroxynicotinic acid, NADH, and *N*-methyl serotonin were obtained
124 from Aladdin (Shanghai, CN). Nicotinic acid mononucleotide was purchased from Macklin
125 (Shanghai, CN). 6-Hydroxy-2-oxo-1,2-dihydropyridine-3-carboxylic acid was from Bide
126 (Hunan, CN). 2,3-Butanedione was from Alfa (Zhengzhou, CN). Total bile acid (TBA) ELISA
127 kit was purchased from Aidisheng (Yancheng, CN). Water was purified by employing a Milli-
128 Q® water system (Millipore, Billerica, MA, USA).

129 **2.2. Animal Model for Fibrosis-Associated Hepatocellular Carcinoma**

130 Liver cancer staging was studied by the diethylnitrosamine-carbon tetrachloride (DEN-
131 CCl_4) chemical-induced mouse model of fibrosis and inflammation-associated HCC since liver
132 fibrosis was not featured in most cancer models in rodents [21]. All animal experiments and
133 study protocols were approved by the University of Hong Kong (HKU)'s Committee on the
134 Use of Live Animals in Teaching and Research (CULATR), in accordance with the Animals
135 (Control of Experiments) Ordinance of Hong Kong. Mice were sacrificed if body weight loss
136 exceeded 20%, and the maximal tumor burden allowed was not exceeded. C57BL/6J mice from
137 the Chinese University of Hong Kong were acclimatized for 1 week at 22 ±2 °C and 60 ±5%
138 relative humidity under a 12-hour light/dark cycle.

139 To develop the animal model, briefly, a single injection of a low dose of DEN (5 mg/kg) into
140 the 2-week-old C57BL/6 male mice intraperitoneally, a well-known model of liver
141 carcinogenesis [22]. Repeated administration of a low dose of CCl_4 (0.5 mL/kg), a pro-
142 fibrogenic agent, was begun at the 12th week of biweekly till the 18th week of age. The
143 continuous exposure to CCl_4 triggered the development of hepatic fibrosis and compensatory
144 cell proliferation [23]. As the sampling plan presented in **Table A1**, liver and serum samples of
145 12 healthy mice, 12 fibrosis mice, 12 fibrosis age-matched control (AMC) mice, 12 cirrhosis
146 mice, 12 cirrhosis AMC mice, 12 HCC mice, and 12 HCC AMC mice were harvested at the
147 18th week, 20th week, 20th week, 28th week, 28th week, 47th week, and 47th week respectively.
148 Liver tissue and serum samples were subsequently stored at −80 °C.

149 **2.3. Preparation of Liver and Serum Extracts for Metabolomics**

150 The whole pre-treatment was carried out at 4 °C. In brief, 25 mg of dissected mouse livers
151 were sampled from the same region weighed and transferred into a 1.5-mL centrifuge tube.
152 Three stainless steel beads and 1 mL of iced ice-cold 8:2 ACN/water were added to homogenize
153 the sample by using a bullet blender homogenizer. The tissue homogenate was then

154 centrifugated at 17,000 × g for 10 min and transferred into the new 1.5-mL centrifuge tube.
155 Alternatively, for 100 μL of serum, 400 μL of chilled ACN was added, and the mixture was
156 then centrifugated and transferred into the new centrifuge tube. Subsequently, the aqueous
157 extracts were dried with an IR concentrator (NB-504CIR, N-Biotek MAX-UP, Korea). Dried
158 samples were reconstituted by 200 μL of 1:1 MeOH/water and were mixed well thoroughly by
159 vortex for 1 min. The pooled quality control (QC) sample was prepared by pooling 80 μL of
160 each sample solution together and mixing. All sample solutions and QC sample were stored at
161 –20 °C until analysis.

162 **2.4. UHPLC/HRMS-Based Untargeted Metabolomics**

163 The pre-treated tissue samples were determined by an Ultimate 3000 UHPLC system
164 coupled with a Orbitrap Exploris 120 mass spectrometer (OE120, Thermo Fisher Scientific,
165 San Jose, CA, USA). An ACQUITY UPLC® HSS T3 column (100 mm × 2.1 mm i.d., 1.8 μm,
166 Waters Corporation, Manchester, UK) was used for the chromatographic separation, which was
167 eluted at a constant flow rate of 0.300 mL/min using a gradient elution program with 0.1% of
168 formic acid in water (A) and 0.1% of formic acid in ACN (B) as the mobile phase. The gradient
169 elution program was as follows: 0 min, 2.0% of B; hold 1 min; 19 min, 100.0% of B; hold 2
170 min; back to 2% of B in 0.1 min and held for 4.9 min. The total run-time was 25 min, and the
171 position of divert valve was set as to waste drain during the first half minute. Column
172 temperature and autosampler temperature were set as 30 °C and 10 °C throughout the analysis,
173 respectively. MS data was acquired by using the Xcalibur software and in positive or negative
174 electrospray (ESI) mode separately using the optimized ionization source parameters (spray
175 voltage: 3.0 kV for positive ESI and 2.5 kV for negative ESI; sheath gas: 50 units; auxiliary
176 gas: 12 units; sweep gas: 0 unit; ion transfer tube temperature: 320 °C; vaporizer temperature:
177 350 °C). The mass spectrometer was operated in the full-scan mode from the mass-to-charge
178 ratio (*m/z*) values of 70–1,000, and the LC/MS data was collected in profile mode at resolution
179 of 60,000 (FWHM at *m/z* 200). Untargeted metabolomics data were pre-processed and analyzed
180 on RStudio 2023.12.1+402 (R version 4.3.3). For level 1 identification confidence, the software
181 *TidyMass* was employed to match the *m/z* values of molecular ion and fragments, as well as
182 retention times (RTs) with referenced values recorded in an in-house database [24]. Level 2B
183 annotations were achieved using the embedded external spectral library provided. The scripts
184 can be found at https://github.com/TommyNHL/multiomics4LiverFIBHCCProj.

185 **2.5. Targeted Metabolomics on the UHPLC/ESI-QqQ-MS/MS Platform**

186 The pre-treated tissue samples were determined by an Ultimate 3000 UHPLC system
187 coupled with a TSQ Quanitica™ triple-quadrupole mass spectrometer (Thermo Fisher

188 Scientific, San Jose, CA, USA). The chromatographic conditions were set as same as the
189 conditions of untargeted metabolomics. MS data was acquired by using the Xcalibur software
190 and in positive or negative ESI mode separately for different compound metabolites as **Table**
191 **A2**. The optimized ionization source parameters include: spray voltage, 3.5 kV, static; sheath
192 gas, 35 units; auxiliary gas, 10 units; sweep gas, 1 unit; ion transfer tube temperature, 350 °C;
193 and vaporizer temperature, 320 °C. The mass spectrometer was run in multi-reaction
194 monitoring (MRM) mode, and the optimal collision energy for all the selected compounds was
195 screened from 5 to 45 V as the MRM transitions settings shown in **Table A2**.

196 **2.6. LC/MS-Based Lipidomics**

197 Similar to metabolomics, 25 mg of dissected organs were homogenized and centrifugated in
198 1 mL of iced ice-cold 8:2 ACN/water. Alternatively, for 100 μL of serum, 400 μL of chilled
199 ACN was mixed and centrifugated. Lipids in the mixture were extracted by an addition of 450
200 μL chloroform and 150 μL water. After vortex for 1 min and centrifugation at 12,000 × g for 5
201 min at 6 °C, 450 μL of the upper aqueous layer was transferred into the new 1.5-mL centrifuge
202 tube. Subsequently, the aqueous extracts were dried and reconstituted by 200 μL of 65:30:5
203 ACN/IPA/H_2O, mixing well thoroughly by vortex for 1 min. The pooled QC sample was
204 prepared by pooling 80 μL of each sample solution together and mixing. All sample solutions
205 and QC sample were stored at –20 °C until analysis.

206 The pre-treated biological samples were analyzed by an Ultimate 3000 UHPLC system
207 coupled with OE120. An ACQUITY UHPLC BEH C18 column (100 mm × 2.1 mm i.d., 1.7
208 μm, Waters Corporation, Manchester, UK) was used for the chromatographic separation, which
209 was eluted at a constant flow rate of 0.260 mL/min using a gradient elution program with 0.1%
210 of formic acid in 6:4 ACN/H_2O with 10 mM ammonium formate (A) and 0.1% of formic acid
211 in 9:1 IPA/ACN with 10 mM ammonium formate (B) as the mobile phase. The gradient elution
212 program was as follows: 0 min, 30.0% of B; hold 1 min; 2 min, 45.0% of B; 7 min, 70.0% of
213 B; hold 2 min; 17 min, 100.0% of B, hold 2 min, back to 30% of B in 1.0 min and held for 5.0
214 min. The total run-time was 25 min, yet the position of divert valve was set as to waste drain
215 during the first half minute. The temperatures of column and autosampler were set as 55 °C and
216 18 °C throughout the analysis, respectively. MS data was acquired by using the Xcalibur
217 software and in positive or negative ESI mode separately using the optimized ionization source
218 parameters (spray voltage: 3.0 kV for positive ESI and 2.5 kV for negative ESI; sheath gas: 40
219 units; auxiliary gas: 10 units; sweep gas: 0 unit; ion transfer tube temperature: 320 °C; vaporizer
220 temperature: 350 °C). The mass spectrometer was run in the $ddMS^2$ mode with HCD collision
221 energies of 25 and 30% from the *m/z* values of 100–1,500, and the LC/MS data was collected

222 in profile mode at resolution of 60,000 for MS^1 and 15,000 for MS^2 (FWHM at *m/z* 200). Level
223 2B annotations of lipids were achieved using LipidSearch (Thermo Fisher Scientific, San Jose,
224 CA, USA). In LipidSearch, a lipid defined as grade A indicates that all fatty acid (FA) chains
225 belonging to a given lipid were completely identified, while grade C indicates the detection of
226 lipid class-specific ions or FA-derived product ions. A python v.3.11 scripts were written for
227 alignment and pooling lipids by class on Jupyter Notebook (Anaconda3). The scripts can be
228 found at https://github.com/TommyNHL/multiomics4LiverFIBHCCProj.

229 **2.7. Total Bile Acid Content**

230 Cold-chilled absolute EtOH was added to 60 mg of mouse liver tissue in a 1.5-mL centrifuge
231 tube. to homogenize the sample by using a bullet blender homogenizer. After vortex for 1 min
232 and centrifugation at 12,000 × g for 10 min at 4 °C, 10 μL of the supernatant was sampled into
233 a transparent 96-well plate. Sample in each well was mixed with the reagents provided by
234 vendor, pre-treated and analyzed by ELISA reader following the manufacturer's protocols
235 provided. The concentration of TBA content is presented by nmol of TBA per gram of tissue
236 sample (nmol/g).

237 **2.8. Global Transcriptomics by RNA Sequencing**

238 RNA sequencing (RNA-Seq) was performed for 6 animal subjects in each fibrosis, cirrhosis,
239 HCC, and their AMCs groups. The 20 mg of non-tumor regions of mouse liver were subjected
240 to total RNA extraction using the Trizol® reagent (Life Technologies, NZ). Each tissue sample
241 was placed in 1 mL of the Trizol solution and homogenized.using a PRO200 homogenizer (Pro
242 Scientific, CT, USA). The homogenization was carried out in two 20-second bursts at 30,000
243 rpm, with the sample kept on ice during the intermittent periods. Chloroform was added to the
244 Trizol-tissue mixture, and the samples were centrifuged to separate the aqueous phase
245 containing the extracted RNA. The RNA was then precipitated by the addition of IPA, and the
246 precipitate was washed with 75% EtOH, dried, and resuspended in RNase/DNase-free water.
247 Sample pretreatment processes to purify and fragment mRNA, synthesize first and second
248 strand cDNA, ligate adapters, enrich DNA fragments, and short-read by 2 × 150 bp followed
249 the high-throughput protocol of Illumina TruSeq™ RNA Library Prep Kit. RNA-Seq data were
250 pre-processed and analyzed on RStudio 2023.12.1+402 (R version 4.3.3). The scripts can be
251 found at https://github.com/TommyNHL/multiomics4LiverFIBHCCProj.

252 **2.9. Statistical Analysis and Data Visualization**

253 Python v.3.11 on Jupyter Notebook (Anaconda3), R version 4.3.3 on RStudio
254 2023.12.1+402, and Microsoft Excel 2024 were used for statistical analyses and data
255 visualization. Results were expressed as mean ± standard deviation (SD). Student's *t*-test was

256 used to assess statistically significant differences between the disease group and its AMC group,
257 by which a value of $p \leq 0.10$ was considered as statistically significant.

258 **3. Results**

259 **3.1. Untargeted Metabolomics and Global Transcriptomics Identify Hepatic Fibrosis-**
260 **Cirrhosis-HCC Progression-Related Metabolic Pathways.**

261 We initiated our study by untargeted multi-omics analyses, including reverse-phase liquid
262 chromatography/mass spectrometry (RPLC/MS)-based metabolomics and RNA-Seq, to
263 discover the main metabolic disturbances that occur during the progression from liver fibrosis
264 to cirrhosis and eventual HCC using the DEN-CCl_4 mouse model. At each disease stage, omics
265 data of the diseased mice were evaluated against the data of age-matched controls (AMCs). For
266 metabolite identification at this point, the confidence level followed the criteria of level 2B of
267 the Metabolomics Standards Initiative [25], implying that the mass-to-charge ratio (*m/z*) values
268 of the annotated metabolites' molecular ions were matched with the chemical standards' values
269 registered in mass spectral libraries. A collection of annotated metabolites exhibited disease
270 stage-specific significant differences and fold changes compared to their corresponding AMCs
271 **(Figure 1A,B)**, including lipids. Notably, their altered levels were not due to any systematic
272 error during LC/MS assay, as all injections for quality control (QC) in both positive **(Figure**
273 **1A)** and negative **(Figure 1B)** electrospray ionization (ESI) mode were assessed to have
274 tolerable relative standard derivations (RSDs) of <30% [26].

275 Metabolite set enrichment analyses on the untargeted metabolomics data showed a list of
276 pathways were significant and agreed with the pathway enrichment results of RNA-Seq **(Figure**
277 **2A,B)**. Several significant pathways (i.e., AAG metabolism, tryptophan metabolism, and citrate
278 cycle) in fibrosis **(Figure 2A,B)** were also discriminative in cirrhosis **(Figure 2C)** and HCC
279 **(Figure 2D)**. Together with nicotinate/nicotinamide metabolism **(Figure 2C,D)**, they were all
280 NAD^+- or energy metabolism -related pathways. Targeted metabolomics was then performed
281 to relatively quantify these compound metabolites in bulk liver tissue samples and serum,
282 accompanied by lipidomics since FA metabolism was also enriched in global transcriptomics
283 and relevant to energy metabolism **(Figure 2B)**.

284 **3.2. Integration of Targeted Metabolomics and RNA Sequencing Reveals Decreased**
285 **Hepatic Nicotinamide Levels Despite Upregulation of *De Novo* NAD^+ Synthesis.**

286 To further explore the disturbances in NAD^+ metabolism identified in the untargeted
287 analyses, we performed targeted RPLC/tandem MS on rodent liver tissue samples. This
288 revealed the metabolites of the kynurenine pathway of tryptophan metabolism were

289 significantly increased in fibrotic livers **(Figure 3A,B)**. Transcriptomic analysis showed that all
290 the genes encoding regulatory enzymes were significant upregulated as differentially expressed
291 gene (DEGs) during fibrogenesis **(Figure 3A and Table A1)**, especially the overexpression of
292 the rate-limiting enzyme tryptophan 2,3-dioxygenase (*Tdo2*). This finding aligns with the
293 results of tryptophan-kynurenine pathway upregulation reported by Hoshi *et al.* in their CCl_4-
294 induced fibrotic mouse livers [27].

295 Our targeted analysis also indicated a continuous, significant decrease in hepatic
296 nicotinamide (NAM) levels across the fibrosis-cirrhosis-HCC disease progression **(Figure**
297 **3A,C)**, despite a significant upregulation of the *de novo* NAD^+ synthesis pathway **(Figure 3A–**
298 **C)**. The RNA-Seq data for fibrosis agreed with the depletion of the available hepatic NAM pool,
299 which was attributed to the increased expression of the NAM *N*-methyltransferase (*Nnmt*) gene
300 **(Table A1)**, catalyzing the methylation of NAM and resulting in a significant increase of the
301 downstream end-product *N*-methyl-4-pyridone-3-carboxamide **(Figure 3A,C)**. Furthermore,
302 we overserved downregulation of genes encoding the Sirtuin (SIRT) family of NAD^+-
303 dependent deacetylases, as well as the rate-limiting enzyme NAM phosphoribosyltransferase
304 (*Nampt*) in the NAD^+ salvage pathway. In contrast, the expression of NAM mononucleotide
305 adenylyltransferase 1 (*Nmnat1*), which catalyzes the final step of *de novo* NAD^+ synthesis, was
306 upregulated. The association between the imbalance of NAM consumption/salvage and liver
307 fibrosis via SIRT and NAD^+ metabolism, as reported by Komatsu *et al.* [28], consolidates our
308 findings on the nicotinate and NAM metabolism.

309 **3.3. Rewiring of NAD^+ Metabolism Dysregulates NAD^+-Dependent Pathways.**

310 The observed disturbances in NAD^+ homeostasis, driven by the depletion of the salvage
311 pathway substrate NAM, prompted us to further investigate the downstream impact on NAD^+-
312 dependent pathways, including FA metabolism, citrate cycle, and AAG metabolism, during the
313 fibrosis-associated HCC progression [29]. Our targeted metabolomics and lipidomics analyses
314 revealed significant upregulation of FA beta-oxidation, as evidence by the progressive decrease
315 of the free medium-chain saturated FA (9:0) and long-chain saturated free FAs, palmitate and
316 stearate, and the increase in the acylcarnitine pool level **(Figure 3A,D)**. The transcriptomics
317 data indicated an increased expression of a cascade of DEGs encoding enzymes involved in FA
318 oxidation (FAO) **(Figure 3A and Table A1)**, including the rate-limiting enzymes carnitine
319 palmitoyltransferase 1A (*Cpt1a*), suggesting a shift towards the utilization of straight-chain free
320 FAs as an energy source [30]. Moreover, we observed significantly increased levels of
321 asparagine, aspartate, glutamine, and glutamate in the AAG metabolism pathway **(Figure**
322 **3A,E)** and a slightly upregulation of most citrate cycle intermediates **(Figure 3A,F)**. The RNA-

323 Seq data showed that all the related DEGs were significantly overexpressed in these metabolic
324 pathways, corroborating the alterations observed in the targeted metabolomics data. Our
325 findings of increased hepatic acylcarnitine and elevated TCA cycle activity were collectively
326 aligned with the results reported by Satapati *et al.*, which demonstrated that mitochondrial
327 citrate cycle anaplerosis was dysregulated by the upregulation of gluconeogenesis in high-fat
328 diet male mice with obesity and hepatic insulin resistance [31].

329 **3.4. Several Potential Diagnostic Tissue and Serum Metabolite Biomarkers Are Suggested**
330 **for Disease Monitoring or Detection.**

331 The integration of the targeted metabolomics and transcriptomics data, along with the
332 comparative analysis of liver tissue and serum samples, allowed us to identify several potential
333 diagnostic biomarkers that could be feasible for monitoring the progression of liver disease.
334 Our analyses revealed the upregulation of serotonin and indoleacetate **(Figure 3B)**, the
335 depletion of NAM, and the increase of quinolinate, *N*-methyl-4-pyridone-3-carboxamide
336 **(Figure 3C)**, the consumption of straight-chain FAs, the accumulation of acylcarnitine level,
337 ceramide level **(Figure 3D)**, glutamate **(Figure 3E)**, as well as the citrate cycle intermediates
338 like 2-oxo-glutarate, malate, and fumarate **(Figure 3F)** exhibited progressive alterations along
339 the continuum of fibrosis-cirrhosis-HCC. These tissue biomarkers thus have the potential for
340 translational application through fine-needle aspiration biopsy assessment.

341 As primary bile acid (BA) biosynthesis was also one of the significant pathways in fibrosis-
342 associate HCC progression **(Figure 2A,C,D)**, primary BAs were analyzed in rodent samples.
343 Taurochenodeoxycholate and taurocholate showed progressive increases at each disease stage
344 in the DEN-CCl_4 mice **(Figure A1A)**. Among the detectable BAs, chenodeoxycholate showed
345 significant difference from the controls in the HCC stage in rodent samples but not
346 progressively changed in the rodent samples **(Figure A1A,B)**. The total BA content showed no
347 significant changes at each stage **(Figure A2)**. Serum BAs also showed no predictable pattern
348 along the fibrosis-associated HCC progression. Chenodeoxycholate, cholate,
349 glycochenodeoxycholate, and glycocholate only indicated stage-specific significances **(Figure**
350 **A1C)**. Despite the lack of discovery of novel serum BA biomarkers, our result of glycocholate
351 increment was in agreement with the previously reported data from another group [32].

352 Besides serum BAs, we identified potential serum metabolite biomarkers with progressive
353 changes that could provide a relatively non-invasive approach for early diagnosis **(Figure 4A–**
354 **C)**, such as the decreased levels of 5-hydroxytryptophan and serotonin **(Figure 4B)**, and the
355 elevated level of quinolinate **(Figure 4C)**. High level of serum quinolinate has been found in
356 liver cirrhosis patients with systematic inflammation [33]. Tryptophan, which was proposed as

357 a potential serum biomarker by previous reports on the perturbations of tryptophan metabolism
358 during hepatic fibrosis progression in rodent models [32], was altered with progressive increase
359 along fibrosis-cirrhosis-HCC staging, if its relative intensity to the AMC at each disease stage
360 is neglected.

361 **3.5. Disturbances in NAD^+ Homeostasis and Its Associated Pathways Trigger Pro-**
362 **Inflammatory Consequences.**

363 The disturbances in NAD^+ homeostasis and the associated dysregulation of NAD^+-
364 dependent pathways during liver disease progression prompted us to further investigate the
365 potential pro-inflammatory consequences using data from the transforming growth factor beta
366 1 (TGF-β1)-activated human HSC cell line LX-2 cell [34]. This is because the activation of
367 HSCs, which involves the transformation of quiescent cells into proliferative, matrix-producing
368 myofibroblasts, is recognised as a pivotal mechanism driving fibrosis in both experimental and
369 clinical liver disease models [35]. Our transcriptomic analysis of the bulk rodent liver samples
370 and TGF-β1-stimulated LX-2 cells revealed that the upregulation of tryptophan metabolism and
371 serotonin synthesis may not be located within the HSCs, or the expression patterns may be
372 temporally dissociated **(Figure 5A)**. The NAD^+ metabolism dysregulation appears to occur at
373 an earlier stage, while the tryptophan pathway upregulation could be a later adaptive response
374 during liver fibrogenesis. In the activated LX-2 cells, the overexpression of the DEGs, including
375 3-hydroxyanthranilate (3-HAA) 3,4-dioxygenase (*Haao*), quinolinate phosphoribosyl
376 transferase (*Qprt*), *Cd38*, and nuclear factor kappa B subunit 1 (*Nfkb1*), was consistent with the
377 RNA-Seq data from our *in vivo* studies **(Figure 5A,B,D,F and Table A1)**. Also, the
378 downregulated genes in the *in vitro* studies, such as the AMPK regulatory subunit 5'-AMP-
379 activated protein kinase subunit gamma-2 (*Prkag2*), *Nnmt*, *Sirt1*, and aldehyde oxidase 1 (*Aox1*),
380 were also identified as the DEGs in the rodent fibrotic liver samples **(Figure 5A–C,E and**
381 **Table A1)**.

382 In the HSCs, the overexpression of *Nnmt*, which catalyzes the methylation of NAM, led to
383 the accumulation of *N*1-methyl NAM. This NAM depletion was further exacerbated by the
384 downregulation of *Aox1* **(Figure 5A–C,E and Table A1)**. The decreased NAM availability was
385 intensified by the downregulation of *Sirt1* and AMPK/PRKAG2, leading to impaired NAM
386 salvage. The reduced *Sirt1* activity also diminished the silencing of pro-inflammatory NF-κB
387 signaling. Together with the upregulation of CD38, the inactivation of AMPK promoted the
388 activation of pro-inflammatory pathways. Notably, PRKAG2 variants have been associated
389 with liver cirrhosis [36], and 3-HAA has been reported to regulate inflammasome activation
390 [37], further supporting our collective findings.

391 **3.6. Downregulated AMPK Signaling Pathway Triggers Lipid Homeostasis Imbalance.**

392 Our metabolite set enrichment analyses revealed that the sphingolipid metabolism pathway
393 was significantly perturbed in the early stages of fibrosis and cirrhosis **(Figure 2A,C)**. The
394 differential expression of key genes involved in the ceramide biosynthetic pathway was notably
395 upregulated **(Figure 3A,D and Table A1)**. Meanwhile, the significant differences in
396 acylcarnitine, a marker of FAO, relative to the levels in the AMCs was also observed **(Figure**
397 **3A,D)**, suggesting a strong propensity for FA catabolism. This is supported by the evidence that
398 the presence of *Cpt1a*, the rate-limiting enzyme in beta-oxidation, is crucial for the activation
399 of HSCs [30]. Elevated expression of *Cpt1a* was reported in the HSCs of patients with
400 non-alcoholic steatohepatitis (NASH), along with a positive correlation with the hepatic
401 fibrosis score [30]. Upon activation, HSCs begin to lose their intracellular FA stores.
402 Interestingly, the expression of *Cpt1a* was downregulated in the TGF-β1-stimulated LX-2 cells
403 after 24 hours of incubation **(Table A1)**, contrasting with its upregulation during the earlier
404 stages of activation (from 1 to 12 hours of incubation) reported by Fondevila *et al.* [30]. Our
405 transcriptomic analysis of the bulk rodent liver samples and *in vitro* studies revealed that the
406 upregulation of FAO may be temporally dissociated **(Figure 6A)**, occurring at an earlier stage,
407 while the steroid biosynthesis upregulation could be a later adaptive response during liver
408 fibrogenesis.

409 In the activated HSCs, the overexpression of the DEGs, including ATP citrate lyase (*Acly*)
410 and FA synthase (*Fasn*) in *de novo* lipogenesis (DNL), acyl-CoA:cholesterol acyltransferase 2
411 (*Acat2*), 3-hydroxy-3-methylglutaryl-CoA synthase 1 (*Hmgcs1*), sterol regulatory element-
412 binding protein 2 (*Srebf2*), and a cascade of genes in the mevalonate pathway of
413 cholesterogenesis, including 3-Hydroxy-3-methylglutaryl-CoA reductase (*Hmgcr*), was
414 consistent with the RNA-Seq data from our *in vivo* studies **(Figure 6A,B,D,F and Table A1)**.
415 Both *in vivo* and *in vitro* studies showed the downregulations of the AMPK-SIRT1 axis and the
416 consequent derepression of the sterol regulatory element-binding proteins (SREBPs), which are
417 key transcriptional regulators of DNL and cholesterogenesis in HSCs **(Figure 6A–C,E and**
418 **Table A1)** [38]. This resulted in the overexpression of genes *Acly* and *Fasn*, as well as those
419 involved in cholesterol biosynthesis, in line with the fact that lipogenesis required the
420 overexpression of the rate-limiting enzyme *Fasn* in mouse models of obesity and NAFLD [39].

421 **4. Discussion**

422 In this comprehensive multi-omics study, we have revealed the major metabolic pathways
423 and signaling networks that are dysregulated during liver fibrosis and inflammation-associated

424 HCC progression. The integration of untargeted metabolomics, targeted metabolomics,
425 lipidomics, and global transcriptomics has provided a holistic understanding of the metabolic
426 rewiring that occurs in the early stages of liver fibrogenesis. The key metabolic pathways
427 identified to be dysregulated include NAD^+ metabolism, *de novo* NAD^+ biosynthesis,
428 sphingolipid synthesis, FAO, DNL, and cholesterogenesis. Global transcriptomics in our *in vivo*
429 studies validates the metabolic alterations by DEGs expression. The DEGs are double
430 confirmed by the external RNA-Seq data of TGF-β1-treated LX-2 cells [34].

431 The importance of NAD^+ metabolism in regulating various cellular processes is well-
432 established [29], and our study has revealed its significant dysregulation during liver disease
433 progression. The state-specific changes in the levels of NAD^+ and its precursor, NAM, suggest
434 a complex interplay between *de novo* NAD^+ synthesis, NAM salvage, and NAM clearance
435 mechanisms. In the early stages of HCC progression (i.e., advanced fibrotic liver stages in
436 fibrosis and cirrhosis), despite the upregulation of *de novo* NAD^+ synthesis, the hepatic NAM
437 levels were decreased **(Figure 3A,C)**. This was due to the overexpression of *Nnmt* **(Figure
438 5A,B,D,F and Table A1)**, catalyzing the methylation of NAM. The overexpression of *Nnmt*
439 was found during the progression of various cancers [40]. Its correlation to the cancer-
440 associated fibroblast was reported [41], yet our *in vitro* analysis demonstrated a comparative
441 overexpression of the DEGs encoding NAD^+ metabolism in the activated HSCs, implying *Nnmt*
442 has a central role of metabolic regulation of myofibroblast differentiation and cancer
443 progression [41].

444 The accumulation of methylated NAM was exacerbated by the downregulation of *Aox1*
445 **(Figure 5A–C,E and Table A1)**, an enzyme responsible for the clearance of this methylated
446 metabolite. As a "methyl sink" in carcinogenesis, NAM is methylated and eventually excreted
447 from the body [42]. Measurements of serum and urine methylated NAM was found to be
448 significantly higher concentrations in patients with cirrhosis compared to healthy controls [43],
449 suggesting that the impairment in NAM salvage mechanisms leads to the excessive clearance
450 of this methylated metabolite from the body and decreased NAD^+ salvage.

451 Attempted recovery of NAM and NAD^+ was attained by the upregulation of the *de novo*
452 NAD^+ synthesis. It was evidenced by a study on the depressed expression of NAM salvage in
453 mice [44]. Overexpression of *Haao* and *Qprt* were found in the HSCs **(Figure 5A,B,D,F and
454 Table A1)**. This enzymatic upregulation led to the rapid production and consumption of
455 quinolinate **(Figure 3A,C,4A)**, suggesting a metabolic adaption to maintain hepatic NAD^+
456 levels. Upregulation of tryptophan-kynurenine pathway in liver was also reported in the
457 consequence of hypoxia-causing manganese exposure [45]. Despite the increased hepatic

458 NAD^+ level observed **(Figure 1A,C)**, the system was unable to compensate for the loss of NAM,
459 as the NAD^+ could not be efficiently converted back into NAM due to the downregulation of
460 AMPK/PRKAG2 and SIRT1 **(Figure 5A–C,E and Table A1)**. As a result, the excess NAD^+
461 was shunted into the systemic circulation. Increased serum NAD^+ levels in adults with
462 metabolic diseases, including obesity and NAFLD was reported, and there was no significant
463 interaction between age, sex, drinking, smoking, and NAD^+ for the metabolic diseases [46].
464 The high blood NAD^+ level was not attributed from the non-hepatic NAD^+ [47], suggesting the
465 circulating NAD^+ was contributed by the liver.

466 The decreased hepatic NAM levels, despite the upregulation of *de novo* NAD+ biosynthesis,
467 contributed to the activation of pro-inflammatory signaling cascades in the HSCs through
468 multiple mechanisms. Firstly, the downregulation of the AMPK-SIRT1 axis, resulting from the
469 NAM depletion and NAD^+ affluence, led to the derepression of NF-κB signaling **(Figure**
470 **5A,B,D,F and Table A1)**. While the decreased NAM levels and consequent impairment of this
471 axis allowed for the unchecked activation of NF-κB in the HSCs. Additionally, the increased
472 expression of CD38, being found on the surface of HSCs [48], further exacerbated the pro-
473 inflammatory consequences. NAD^+ affluence has been reported by selectively inhibition of
474 CD38 ectoenzyme, accompanying with significant prevention from fibrosis [49], partially
475 through the mechanisms of blunting the recruitment of immune cells and NF-κB signaling [50].
476 Several studies reported boosting hepatic NAD^+ level improved liver injury and inflammation
477 by nicotinic acid (NA) riboside supplementation [47], or NA supplementation by converting
478 NAM into NAD^+ [51], counteracting the activity of CD38 by that of NAMPT. However,
479 targeting CD38 or upregulating NAMPT resulted to a similar effect as upregulation of
480 tryptophan-kynurenine pathway, and might be not sufficient when AMPK-SIRT1 is still
481 downregulated. Together, targeted interventions aimed at restoring NAM availability,
482 modulating AMPK-SIRT1-NF-κB axis, and inhibiting CD38 activity may hold significant
483 therapeutic potential for mitigating the inflammatory and fibrogenic processes.

484 Besides AMPK-SIRT1-NF-κB axis, our analysis revealed that rewiring of NAD^+
485 metabolism also resulted to imbalance in hepatic lipid homeostasis during the progression of
486 liver disease through AMPK-SIRT1-NF-κB-SREBP axis in HSCs [52]. The activity of
487 SREBP2 was indicated that it can be regulated by 3-HAA metabolism [37]. The key
488 transcription factors involved in this lipid metabolism dysregulation are the SREBPs,
489 which are substrates of SIRT1 enzyme [38]. While the SREBP1a and SREBP1c isoforms
490 (encoded by the *Srebf1* gene) are regulated by the AMPK-SIRT1 axis, the SREBP2
491 isoform (encoded by the *Srebf2* gene) is less susceptible to this repression [53]. We

492 observed the upregulation of key genes involved in the SREBP-regulated pathways of DNL
493 and cholesterol biosynthesis **(Figure 6A,B,D,F and Table A1)**. This suggests a shift towards
494 increased synthesis of palmitate or other FAs, cholesterol, and sterol metabolites. Interestingly,
495 despite this transcriptional upregulation, we detected decreased levels of palmitate and other
496 FAs along the disease progression. This indicated that the overall tendency in FA metabolism
497 was towards the increased acylcarnitine formation and subsequent FAO **(Figure 3A,D)**. This
498 could potentially be for the purpose of other lipid biosynthesis, such the observed upregulation
499 of the sphingolipid signaling pathway **(Figure 3A and Table A1)** and ceramide biosynthesis
500 in the fibrosis and cirrhosis stages.

501 The overexpression of genes encoding FAO, including the rate-limiting enzyme *Cpt1a* was
502 observed *in vivo* **(Figure 3A and Table A1)**. Expression of *Cpt1a* showed to be induced by
503 the FAO-derived reactive oxygen species [30]. In our *in vivo* studies, the FAO appears
504 to be upregulated by the demands of saturated FAs, as reflected by the lipidomics data
505 **(Figure 3A,D)**. Although our *in vitro* data analysis showed the activated HSCs might have a
506 delayed response in FAO, elevated expression of *Cpt1a* is a hallmark in HSC activation in the
507 pathogenesis of hepatic fibrosis in patients with NASH, in rodents, and in TGF-β1-stimulated
508 LX-2 cells incubated with saturated FAs-rich mediation [30]. A study also showed that killer
509 T cells-derived interferon gamma (IFN-γ) induces activation of FAO and *Cpt1a* upregulation
510 in cancer cells in an AMPK-dependent manner [54]. This can be used to explain why *Cpt1a* is
511 observed *in vivo* but not in *in vitro* study, highlighting the importance of the complex liver
512 microenvironment in shaping the metabolic adaptations.

513 Although increasing saturated FA (palmitate and stearate) levels by modulating NAD^+
514 metabolism by NAM mononucleotide or NAM riboside supplementation have shown to
515 ameliorate hepatic metabolic disturbances in mice with NAFLD [55], potential therapeutic
516 strategies to retore lipid homeostasis and mitigate the fibrogenic response should targeted the
517 AMPK-SIRT1-SREBP axis. Approaches that aim to activate AMPK have shown promise in
518 preventing lipogenesis and NAFLD [56]. However, the role of NF-κB in the liver is complex,
519 and its inhibition may have both beneficial and detrimental effects, warranting a cautious
520 approach [57].

521 This comprehensive multi-omics study has revealed the complex dysregulation of NAD^+
522 metabolism and its profound impact on the metabolic and signaling networks during the
523 progression of liver fibrosis and inflammation-associated HCC. The depletion of NAM levels,
524 despite the upregulation of *de novo* NAD^+ biosynthesis, appears to be a critical driver of the
525 pathological changes. This NAM depletion disrupts the AMPK-SIRT1 axis, leading to the

526 aberrant activation of pro-inflammatory NF-κB signaling in the HSCs. Furthermore, the
527 rewiring of NAD^+ metabolism also contributes to the imbalance in hepatic lipid homeostasis
528 through the AMPK-SIRT1-NF-κB-SREBP axis. This study provides valuable insights into the
529 complex metabolic reprogramming that occurs during the various stages of HCC progression,
530 offering new avenues for the development of targeted therapeutic interventions and early
531 diagnosis.
532

533 **Figure Legends**

534 **Figure 1. Untargeted metabolomics of the DEN-CCl_4-treated mice liver with liver**
535 **fibrosis, cirrhosis, and hepatocellular carcinoma.** (A) Mass spectrometry data
536 acquired in positive and (B) negative electrospray ionization mode. Significant
537 metabolites from each disease stage were annotated in level 3 chemical identification
538 confidence with a relative standard deviation (RSD) of <30% among quality control
539 samples (QCs). Data were represented by the ratio of signal intensity of disease group
540 to of control group, z-score normalized to normal livers.

541 **Figure 2. Pathway enrichment for the DEN-CCl_4-treated mice liver with liver**
542 **fibrosis, cirrhosis, and hepatocellular carcinoma.** The discriminative metabolic
543 pathways enriched from (A) metabolomics data and (B) RNA sequencing data for
544 hepatic fibrosis, from (C) metabolomics data for cirrhotic liver, and (D) metabolomics
545 data for carcinogenic liver. The NAD^+-related pathways are highlighted.

546 **Figure 3. Stage-sensitive metabolomic and lipidomic changes along liver fibrosis,**
547 **cirrhosis, and hepatocellular carcinoma.** (A) A summary of the multi-omics data for
548 the fibrotic mouse livers. Upregulated genes and metabolites are red-colored.
549 Downregulated genes and metabolites are blue-colored. Non-measured metabolites are
550 grey-colored. Bold text indicated statistical significance with p-value <0.05. Stage-
551 sensitive alterations in metabolites and lipids in (B) tryptophan metabolism, (C)
552 nicotinate and nicotinamide metabolism, (D) fatty acid metabolism, (E) alanine,
553 aspartate, glutamate metabolism, and (F) citrate cycle. Potential biomarkers are dash-
554 highlighted with red grid lines. *Abbreviations: AMC, Age-matched controls; FIB,*
555 *Fibrosis; CIR, Cirrhosis; HCC, Hepatocellular carcinoma; ^, p <0.1; *, p <0.05; **, p*
556 *<0.01; ***, p <0.001.*

557 **Figure 4. Stage-sensitive metabolomic changes in serum along liver fibrosis,**
558 **cirrhosis, and hepatocellular carcinoma.** (A) A summary of the metabolites in

559 tryptophan-kynurenine pathway and NAD^+ metabolism in the fibrotic mice serum.
560 Upregulated metabolites are red-colored. Downregulated metabolites are blue-colored.
561 Non-measured metabolites are grey-colored. Bold text indicated statistical significance
562 with a p-value of <0.05. Stage-sensitive alterations in metabolites and lipids in (B)
563 tryptophan metabolism, and (C) nicotinate and nicotinamide metabolism. Potential
564 biomarkers are dash-highlighted with red grid lines. *Abbreviations: AMC, Age-matched*
565 *controls; FIB, Fibrosis; CIR, Cirrhosis; HCC, Hepatocellular carcinoma; ^, p <0.1; *,*
566 *p <0.05; **, p <0.01; ***, p <0.001.*

567 **Figure 5. NAD^+ metabolism and *de novo* NAD^+ biosynthesis pathway in hepatic**
568 **stellate cells.** (A) A summary of the genes in *de novo* NAD^+ biosynthesis pathway and
569 NAD^+ metabolism that aligned with the changes with the *in vivo* studies. Upregulated
570 genes are red-colored. Downregulated genes are blue-colored. Bold text indicated
571 statistical significance with a p-value of <0.05. *In vitro* and *in vivo* differentially
572 expressed genes were represented (B) by box plots and (C–F) by volcano plots.
573 *Abbreviations: Ctrl, Experimental control; Treat, TGF-β1-activated human HSC cell*
574 *line LX-2 cells; AMC, Age-matched controls; FIB, Fibrosis; ^, p <0.1; *, p <0.05; **,*
575 *p <0.01; ***, p <0.001.*

576 **Figure 6. *De novo* lipogenesis and cholesterogenesis pathway in hepatic stellate cells.**
577 (A) A summary of the genes in *de novo* lipogenesis and cholesterogenesis pathway that
578 aligned with the changes with the *in vivo* studies. Upregulated genes are red-colored.
579 Downregulated genes are blue-colored. Bold text indicated statistical significance with
580 a p-value of <0.05. *In vitro* and *in vivo* differentially expressed genes were represented
581 (B) by box plots and (C–F) by volcano plots. Serum lipids are dash-highlighted with
582 purple grid lines. *Abbreviations: Ctrl, Experimental control; Treat, TGF-β1-activated*
583 *human HSC cell line LX-2 cells; AMC, Age-matched controls; FIB, Fibrosis; CIR,*
584 *Cirrhosis; HCC, Hepatocellular carcinoma; ^, p <0.1; *, p <0.05; **, p <0.01; ***, p*
585 *<0.001.*
586

587 **Supporting Information**

588 Supporting Information is available from the Wiley Online Library or from the author.
589

Author Contributions

Hiu-Lok Ngan: conceptualization, resources, data curation, writing-original draft preparation, writing - review and editing, visualization. **Jacinth Wing-Sum Cheu:** writing - review and editing, visualization. **Kenneth Kin-Leung Kwan:** writing - review and editing, visualization. **Carmen Chak-Lui Wong:** conceptualization, resources, supervision. **Hong Yan:** conceptualization, resources, writing - review and editing, supervision, project administration, funding acquisition. **Zongwei Cai:** conceptualization, resources, supervision, project administration, funding acquisition. All authors have read and agreed to the published version of the manuscript.

Acknowledgements

H. Y. thanks the Start-up Grant for New Academics – YAN Hong (165520). The authors from Hong Kong Baptist University appreciate the contributions made by C.C.-L. W's team in developing and preparing the animal models.

Ethics Statement

All animal experiments and study protocols were approved by the University of Hong Kong (HKU)'s Committee on the Use of Live Animals in Teaching and Research (CULATR), in accordance with the Animals (Control of Experiments) Ordinance of Hong Kong.

Conflict of Interest Statement

The authors declare that they have no conflicts of interest or personal relationships that could influence the work reported in this paper.

Data Availability Statement

All study data are included in the article and/or supporting information. Processed MS-based metabolomics and lipidomics data and RNA-Seq data are available on Zenodo (see 10.5281/zenodo.17140661).

References

[1] J. Ferlay, M. Ervik, F. Lam, M. Colombet, L. Mery, M. Piñeros, A. Znaor, I. Soerjomataram, F. Bray, Global Cancer Observatory: Cancer Today. Lyon, France: International Agency for Research on Cancer, Lyon, France: International Agency for Research on Cancer 419 (2020). https://gco.iarc.fr/today (accessed: October 2023).

[2] J.M. Llovet, A. Villanueva, A. Lachenmayer, R.S. Finn, *Nat Rev Clin Oncol* **2015**, *12*, 408–424.

[3] H. Sung, J. Ferlay, R.L. Siegel, M. Laversanne, I. Soerjomataram, A. Jemal, F. Bray, *CA Cancer J Clin* **2021**, *71*, 209–249.

[4] The American Cancer Society, Liver cancer early detection, diagnosis, and staging, https://www.cancer.org/content/dam/CRC/PDF/Public/8700.00.pdf (accessed: October 2023).

[5] L. Laursen, *Nature* **2014**, *516*, S3–S4.

[6] G. Fattovich, T. Stroffolini, I. Zagni, F. Donato, *Gastroenterology* **2004**, *127*, S35–S50.

[7] A.G. Singal, H.B. El-Serag, *Clinical Gastroenterology and Hepatology* **2015**, *13*, 2140–2151.

[8] D. Dhar, J. Baglieri, T. Kisseleva, D.A. Brenner, *Exp Biol Med* **2020**, *245*, 96–108.

[9] D.Y. Zhang, S.L. Friedman, *Hepatology* **2012**, *56*, 769–775.

[10] P. Luo, P. Yin, R. Hua, Y. Tan, Z. Li, G. Qiu, Z. Yin, X. Xie, X. Wang, W. Chen, L. Zhou, X. Wang, Y. Li, H. Chen, L. Gao, X. Lu, T. Wu, H. Wang, J. Niu, G. Xu, *Hepatology* **2018**, *67*, 662–675.

[11] M. Lewinska, A. Santos-Laso, E. Arretxe, C. Alonso, E. Zhuravleva, R. Jimenez-Agüero, E. Eizaguirre, M.J. Pareja, M. Romero-Gómez, M.A. Jimenez, M.P. Suppli, F.K. Knop, S.K. Oversoe, G.E. Villadsen, T. Decaens, F.J. Carrilho, C.P. de Oliveira, B. Sangro, R.I.R. Macias, J.M. Banales, J.B. Andersen, *EBioMedicine* **2021**, *73*, 103661.

[12] E. Loftfield, M. Stepien, V. Viallon, L. Trijsburg, J.A. Rothwell, N. Robinot, C. Biessy, I.A. Bergdahl, S. Bodén, M.B. Schulze, M. Bergman, E. Weiderpass, J.A. Schmidt, R. Zamora-Ros, T.H. Nøst, T.M. Sandanger, E. Sonestedt, B. Ohlsson, V. Katzke, R. Kaaks, F. Ricceri, A. Tjønneland, C.C. Dahm, M.J. Sánchez, A. Trichopoulou, R. Tumino, M.D. Chirlaque, G. Masala, E. Ardanaz, R. Vermeulen, P. Brennan, D. Albanes, S.J. Weinstein, A. Scalbert, N.D. Freedman, M.J. Gunter, M. Jenab, R. Sinha, P. Keski-Rahkonen, P. Ferrari, *J Natl Cancer Inst* **2021**, *113*, 1542–1550.

[13] Q. Huang, Y. Tan, P. Yin, G. Ye, P. Gao, X. Lu, H. Wang, G. Xu, *Cancer Res* **2013**, *73*, 4992–5002.

[14] Y. Lu, N. Li, L. Gao, Y.J. Xu, C. Huang, K. Yu, Q. Ling, Q. Cheng, S. Chen, M. Zhu, J. Fang, M. Chen, C.N. Ong, *Cancer Res* **2016**, *76*, 2912–2920.

[15] T. Feng, C. Lai, Q. Yuan, W. Yang, Y. Yao, M. Du, D. Zhong, S. Wang, Q. Yang, J. Shang, Y. Shi, X. Huang, *IScience* **2023**, *26*, 107538.

[16] D. Beyoğlu, S. Imbeaud, O. Maurhofer, P. Bioulac-Sage, J. Zucman-Rossi, J.F. Dufour, J.R. Idle, *Hepatology* **2013**, *58*, 229–238.

[17] J. Chaisaingmongkol, A. Budhu, H. Dang, S. Rabibhadana, B. Pupacdi, S.M. Kwon, M. Forgues, Y. Pomyen, V. Bhudhisawasdi, N. Lertprasertsuke, A. Chotirosniramit, C. Pairojkul, C.U. Auewarakul, T. Sricharunrat, K. Phornphutkul, S. Sangrajrang, M. Cam, P. He, S.M. Hewitt, K. Ylaya, X. Wu, J.B. Andersen, S.S. Thorgeirsson, J.J. Waterfall, Y.J. Zhu, J. Walling, H.S. Stevenson, D. Edelman, P.S. Meltzer, C.A. Loffredo, N. Hama, T. Shibata, R.H. Wiltrout, C.C. Harris, C. Mahidol, M. Ruchirawat, X.W. Wang, *Cancer Cell* **2017**, *32*, 57–70.

[18] M.J. He, W. Pu, X. Wang, X. Zhong, D. Zhao, Z. Zeng, W. Cai, J. Liu, J. Huang, D. Tang, Y. Dai, *Cancer Cell Int* **2022**, *22*, 366.

[19] X. He, M.X. Zhou, C. Cheng, S.S. Li, Y. Gao, Z.T. Ma, X.H. Song, Z.F. Bai, Z.S. Zou, X.H. Xiao, J.B. Wang, Y.W. Lu, *Front Pharmacol* **2022**, *13*, 896198.
[20] S.T. Wu, X.X. Wang, W.B. Xing, F.Y. Li, M. Liang, K.S. Li, Y. He, J.M. Wang, *Front Med (Lausanne)* **2023**, *10*, 1160053.
[21] T. Uehara, I.P. Pogribny, I. Rusyn, *Curr Protoc* **2021**, *1*, e211.
[22] S.D. Vesselinovitch, N. Mihailovich, *Cancer Res* **1983**, *43*, 4253–4259.
[23] R.E. Stowell, A. Vlllasana, K.K. Tsuboi, A. Vlllasana, *Cancer Res* **1951**, *11*, 345–354.
[24] X. Shen, H. Yan, C. Wang, P. Gao, C.H. Johnson, M.P. Snyder, *Nat Commun* **2022**, *13*, 4365.
[25] L.W. Sumner, A. Amberg, D. Barrett, M.H. Beale, R. Beger, C.A. Daykin, T.W.M. Fan, O. Fiehn, R. Goodacre, J.L. Griffin, T. Hankemeier, N. Hardy, J. Harnly, R. Higashi, J. Kopka, A.N. Lane, J.C. Lindon, P. Marriott, A.W. Nicholls, M.D. Reily, J.J. Thaden, M.R. Viant, *Metabolomics* **2007**, *3*, 211–221.
[26] H.L. Ngan, K.Y. Lam, Z. Li, J. Zhang, Z. Cai, *TrAC - Trends in Analytical Chemistry* **2023**, *168*, 117333.
[27] M. Hoshi, Y. Osawa, K. Nakamoto, N. Morita, Y. Yamamoto, T. Ando, C. Tashita, T. Nabeshima, K. Saito, *Toxicology* **2020**, *438*, 152458.
[28] M. Komatsu, T. Kanda, H. Urai, A. Kurokochi, R. Kitahama, S. Shigaki, T. Ono, H. Yukioka, K. Hasegawa, H. Tokuyama, H. Kawabe, S. Wakino, H. Itoh, *Sci Rep* **2018**, *8*, 8637.
[29] N. Xie, L. Zhang, W. Gao, C. Huang, P.E. Huber, X. Zhou, C. Li, G. Shen, B. Zou, *Signal Transduct Target Ther* **2020**, *5*, 227.
[30] M.F. Fondevila, U. Fernandez, V. Heras, T. Parracho, M.J. Gonzalez-Rellan, E. Novoa, B. Porteiro, C. Alonso, R. Mayo, N. da Silva Lima, C. Iglesias, A.A. Filliol, A. Senra, T.C. Delgado, A. Woodhoo, L. Herrero, D. Serra, V. Prevot, M. Schwaninger, M. López, C. Dieguez, O. Millet, J.M. Mato, F.J. Cubero, M. Varela-Rey, P. Iruzubieta, J. Crespo, M.L. Martinez-Chantar, R.F. Schwabe, R. Nogueiras, *J Hepatol* **2022**, *77*, 15–28.
[31] S. Satapati, N.E. Sunny, B. Kucejova, X. Fu, T.T. He, A. Méndez-Lucas, J.M. Shelton, J.C. Perales, J.D. Browning, S.C. Burgess, *J Lipid Res* **2012**, *53*, 1080–1092.
[32] H. Chang, H.Y. Meng, S.M. Liu, Y. Wang, X.X. Yang, F. Lu, H.Y. Wang, *Sci Rep* **2017**, *7*, 11433.
[33] J. Clària, R. Moreau, F. Fenaille, A. Amorós, C. Junot, H. Gronbaek, M.J. Coenraad, A. Pruvost, A. Ghettas, E. Chu-Van, C. López-Vicario, K. Oettl, P. Caraceni, C. Alessandria, J. Trebicka, M. Pavesi, C. Deulofeu, A. Albillos, T. Gustot, T.M. Welzel, J. Fernández, R.E. Stauber, F. Saliba, N. Butin, B. Colsch, C. Moreno, F. Durand, F. Nevens, R. Bañares, D. Benten, P. Ginès, A. Gerbes, R. Jalan, P. Angeli, M. Bernardi, V. Arroyo, *Hepatology* **2019**, *69*, 1686–1701.
[34] J.P. Carson, M.W. Robinson, G.A. Ramm, G.N. Gobert, *Mol Biol Rep* **2021**, *48*, 7677–7688.
[35] T. Tsuchida, S.L. Friedman, *Nat Rev Gastroenterol Hepatol* **2017**, *14*, 397–411.
[36] Z. Beyzaei, F. Ezgu, B. Geramizadeh, A. Alborzi, A. Shojazadeh, *BMC Med Genomics* **2021**, *14*, 33.
[37] M. Berg, K.A. Polyzos, H. Agardh, R. Baumgartner, M.J. Forteza, I. Kareinen, A. Gistera, G. Bottcher, E. Hurt-Camejo, G.K. Hansson, D.F.J. Ketelhuth, *Cardiovasc Res* **2020**, *116*, 1948–1957.
[38] S. Shen, M. Shen, L. Kuang, K. Yang, S. Wu, X. Liu, Y. Wang, Y. Wang, *Pharmacol Res* **2024**, *199*, 107037.
[39] T. Matsukawa, T. Yagi, T. Uchida, M. Sakai, M. Mitsushima, T. Naganuma, H. Yano, Y. Inaba, H. Inoue, K. Yanagida, M. Uematsu, K. Nakao, H. Nakao, A. Aiba, Y. Nagashima, T. Kubota, N. Kubota, Y. Izumida, N. Yahagi, H. Unoki-Kubota, Y.

Kaburagi, S.I. Asahara, Y. Kido, H. Shindou, M. Itoh, Y. Ogawa, S. Minami, Y. Terauchi, K. Tobe, K. Ueki, M. Kasuga, M. Matsumoto, *JCI Insight* **2023**, *8*, e161282.

[40] W. Wang, C. Yang, T. Wang, H. Deng, *Cell Death Dis* **2022**, *13*, 267.

[41] M.A. Eckert, F. Coscia, A. Chryplewicz, J.W. Chang, K.M. Hernandez, S. Pan, S.M. Tienda, D.A. Nahotko, G. Li, I. Blaženović, R.R. Lastra, M. Curtis, S.D. Yamada, R. Perets, S.M. McGregor, J. Andrade, O. Fiehn, R.E. Moellering, M. Mann, E. Lengyel, *Nature* **2019**, *569*, 723–728.

[42] P. Pissios, *Trends in Endocrinology and Metabolism* **2017**, *28*, 340–353.

[43] R. Cuomo, M. Dattilo, R. Pumpo, G. Capuano, L. Boselli, G. Budillon, *J Hepatol* **1994**, *20*, 138–142.

[44] S.J. Mitchell, M. Bernier, M.A. Aon, S. Cortassa, E.Y. Kim, E.F. Fang, H.H. Palacios, A. Ali, I. Navas-Enamorado, A. Di Francesco, T.A. Kaiser, T.B. Waltz, N. Zhang, J.L. Ellis, P.J. Elliott, D.W. Frederick, V.A. Bohr, M.S. Schmidt, C. Brenner, D.A. Sinclair, A.A. Sauve, J.A. Baur, R. de Cabo, *Cell Metab* **2018**, *27*, 667-676.e4.

[45] A.S. Warden, N. Sharma, S. Hutchens, C. Liu, N.R. Haggerty, K.C. Gurol, T. Jursa, D.R. Smith, R.D. Mayfield, S. Mukhopadhyay, *Proc Natl Acad Sci U S A* **2025**, *122*, e2423628122.

[46] Y. Liu, X. Chen, X. Deng, F. Yang, J. Zheng, T. Zhou, L. Xu, X. Xie, Z. Ju, B. Wang, C. Zhang, Y. Zhou, *Front Endocrinol (Lausanne)* **2023**, *14*, 1164788.

[47] W.S. Song, X. Shen, K. Du, C.B. Ramirez, S.H. Park, Y. Cao, J. Le, H. Bae, J. Kim, Y. Chun, N.J. Khong, M. Kim, S. Jung, W. Choi, M.L. Lopez, Z. Said, Z. Song, S.G. Lee, D. Nicholas, Y. Sasaki, J. Milbrandt, D.K. Imagawa, D. Skowronska-Krawczyk, D. Chen, G. Lee, C. Jang, Q. Yang, *Cell Metab* **2025**, *37*, 1499–1514.e4.

[48] A. Balaphas, J. Meyer, C. Gameiro, A. Frobert, M.N. Giraud, B. Egger, L.H. Bühler, C. Gonelle-Gispert, *Cells* **2022**, *11*, 1379.

[49] B. Shi, A. Amin, P. Dalvi, W. Wang, N. Lukacs, L. Kai, P. Cheresh, T.R. Peclat, C.C. Chini, E.N. Chini, W. van Schooten, J. Varga, *Sci Rep* **2023**, *13*, 22085.

[50] Y. Tao, J. Wang, X. Lyu, N. Li, D. Lai, Y. Liu, X. Zhang, P. Li, S. Cao, X. Zhou, Y. Zhao, L. Ma, T. Tao, Z. Feng, X. Li, F. Yang, H. Zhou, *Molecular and Cellular Proteomics* **2023**, *22*, 100510.

[51] M. Dall, A.S. Hassing, L. Niu, T.S. Nielsen, L.R. Ingerslev, K. Sulek, S.A.J. Trammell, M.P. Gillum, R. Barrès, S. Larsen, S.S. Poulsen, M. Mann, C. Ørskov, J.T. Treebak, *Journal of Biological Chemistry* **2021**, *297*, 101388.

[52] M. Yan, Y. Cui, Q. Xiang, *Theranostics* **2025**, *15*, 1715–1740.

[53] N. Koundouros, G. Poulogiannis, *Br J Cancer* **2019**, *122*, 4–22.

[54] Z. Liu, W. Liu, W. Wang, Y. Ma, Y. Wang, D.L. Drum, J. Cai, H. Blevins, E. Lee, S. Shah, P.B. Fisher, X. Wang, X. Fang, C. Guo, X.Y. Wang, *Proc Natl Acad Sci U S A* **2023**, *120*, e2302878120.

[55] J. Zhang, F. Chen, *Biomedicine and Pharmacotherapy* **2024**, *175*, 116701.

[56] A. Woods, J.R. Williams, P.J. Muckett, F. V. Mayer, M. Liljevald, M. Bohlooly-Y, D. Carling, *Cell Rep* **2017**, *18*, 3043–3051.

[57] T. Luedde, R.F. Schwabe, *Nat Rev Gastroenterol Hepatol* **2011**, *8*, 108–118.

762 Untargeted metabolomics, targeted metabolomics, and lipidomics are utilized to analyze tissue
763 and serum samples from a mouse model that represents a continuum of liver fibrosis, cirrhosis,
764 and hepatocellular carcinoma (HCC). This comprehensive approach allows us to identify
765 potential biomarkers for inflammation-associated HCC progression and further validate the
766 relevant discriminative metabolic pathways through transcriptomics analysis of human hepatic
767 stellate cells, which are known to be activated during hepatic fibrosis.
768

769 *Hiu-Lok Ngan,[1] Jacinth Wing-Sum Cheu,[2,3] Kenneth Kin-Leung Kwan,[2,3] Carmen Chak-Lui*
770 *Wong,[2,3] Hong Yan,[1,4,]* Zongwei Cai[1,5,]**
771

772 **Rewired NAD$^+$ metabolism promotes NF-κB-mediated oxidative stress and disrupts lipid**
773 **homeostasis in liver fibrosis progression**
774

775 ToC figure

776 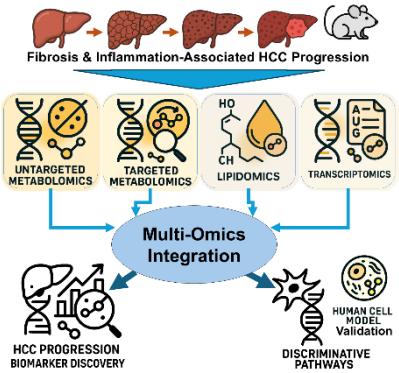

Figure 1

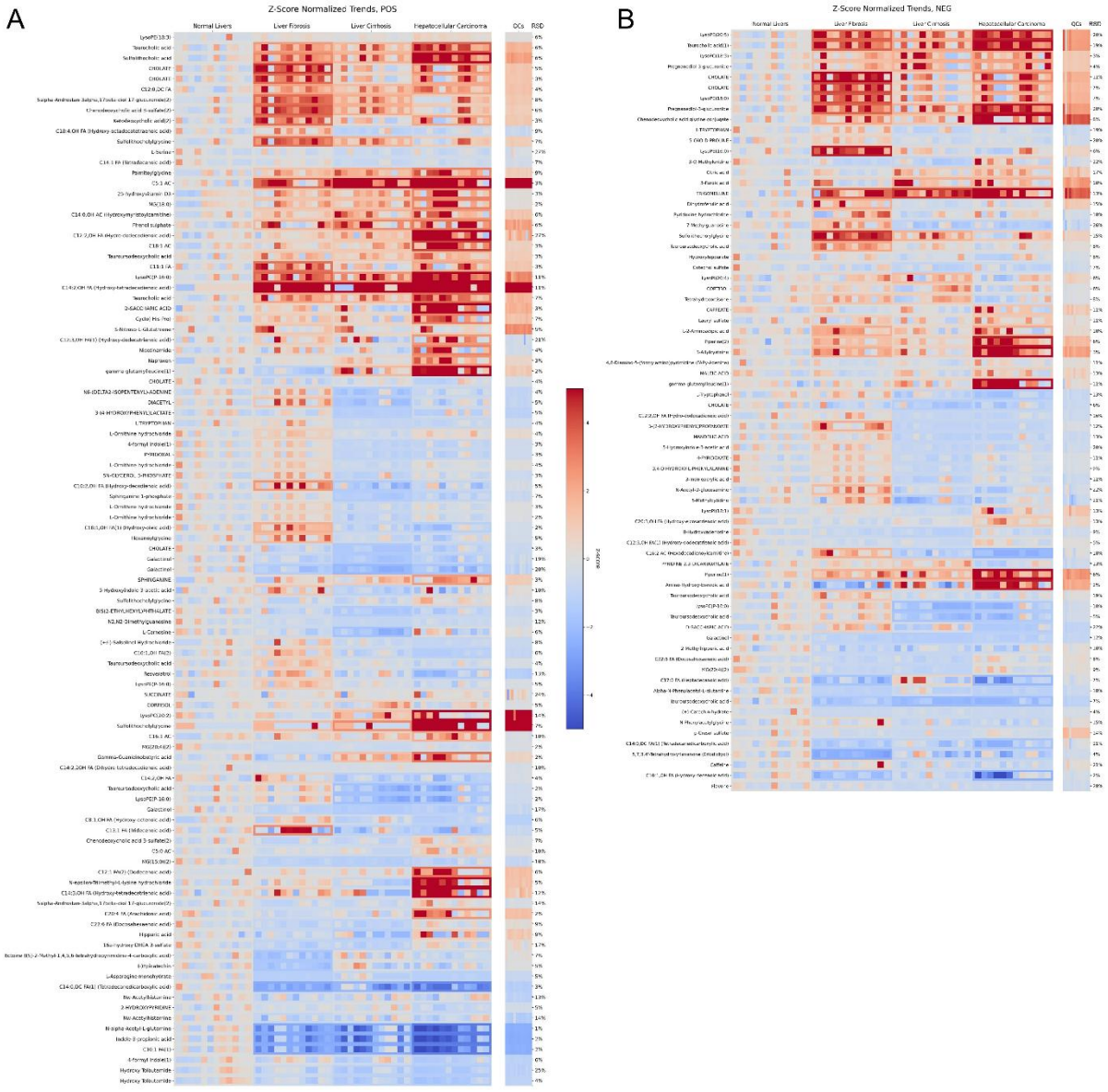
A
Z-Score Normalized Trends, POS
Normal Livers
Liver Fibrosis
Liver Cirrhosis
Hepatocellular Carcinoma
QCs
RSD
B
Z-Score Normalized Trends, NEG
Normal Livers
Liver Fibrosis
Liver Cirrhosis
Hepatocellular Carcinoma
QCs
RSD

Figure 2

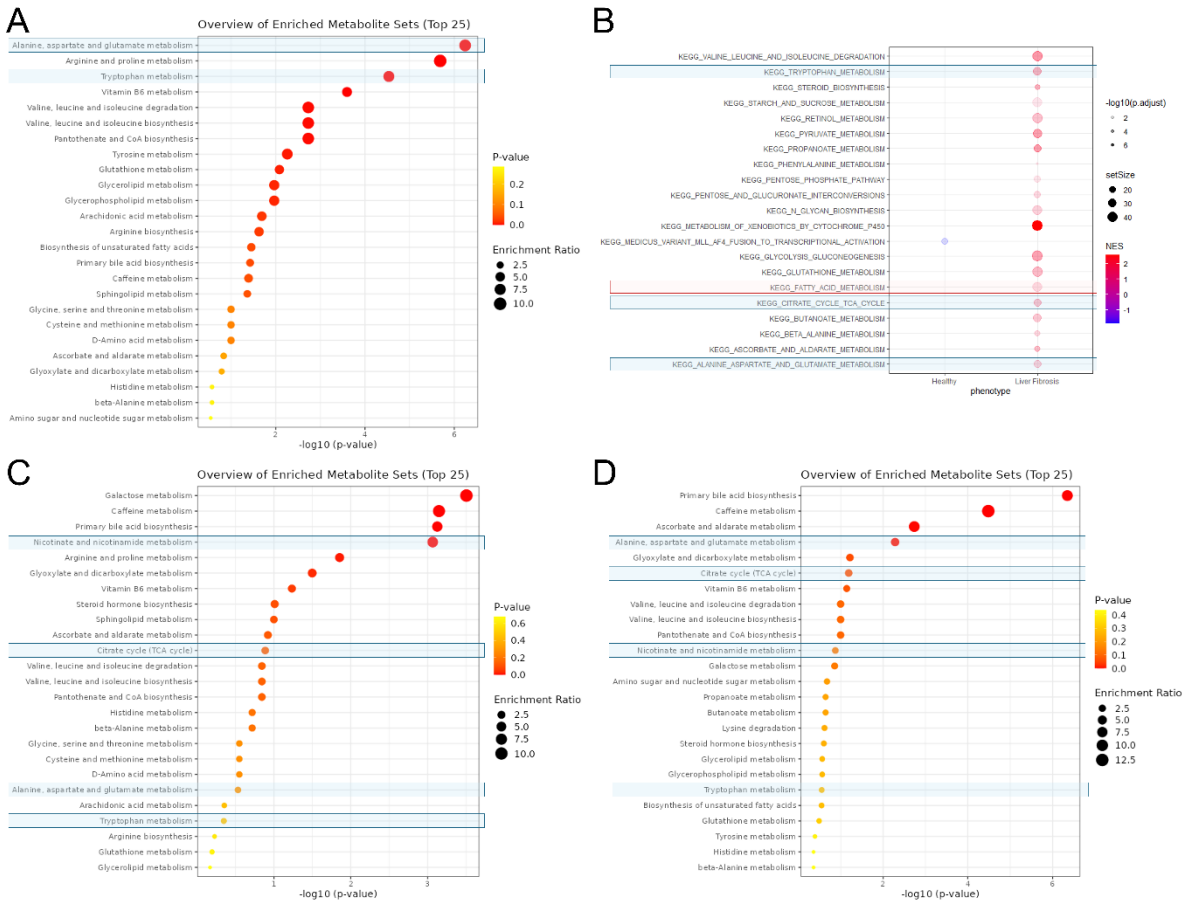
A
Overview of Enriched Metabolite Sets (Top 25)
Alanine, aspartate and glutamate metabolism
Arginine and proline metabolism
Tryptophan metabolism
Vitamin B6 metabolism
Valine, leucine and isoleucine degradation
Valine, leucine and isoleucine biosynthesis
Pantothenate and CoA biosynthesis
Tyrosine metabolism
Glutathione metabolism
Glycerolipid metabolism
Glycerophospholipid metabolism
Arachidonic acid metabolism
Arginine biosynthesis
Biosynthesis of unsaturated fatty acids
Primary bile acid biosynthesis
Caffeine metabolism
Sphingolipid metabolism
Glycine, serine and threonine metabolism
Cysteine and methionine metabolism
D-Amino acid metabolism
Ascorbate and aldarate metabolism
Glyoxylate and dicarboxylate metabolism
Histidine metabolism
beta-Alanine metabolism
Amino sugar and nucleotide sugar metabolism
-log10 (p-value)
P-value
0.2
0.1
0.0
Enrichment Ratio
2.5
5.0
7.5
10.0
B
KEGG_VALINE_LEUCINE_AND_ISOLEUCINE_DEGRADATION
KEGG_TRYPTOPHAN_METABOLISM
KEGG_STEROID_BIOSYNTHESIS
KEGG_STARCH_AND_SUCROSE_METABOLISM
KEGG_RETINOL_METABOLISM
KEGG_PYRUVATE_METABOLISM
KEGG_PROPANOATE_METABOLISM
KEGG_PHENYLALANINE_METABOLISM
KEGG_PENTOSE_PHOSPHATE_PATHWAY
KEGG_PENTOSE_AND_GLUCURONATE_INTERCONVERSIONS
KEGG_N_GLYCAN_BIOSYNTHESIS
KEGG_METABOLISM_OF_XENOBIOTICS_BY_CYTOCHROME_P450
KEGG_MEDICUS_VARIANT_MLL_AF4_FUSION_TO_TRANSCRIPTIONAL_ACTIVATION
KEGG_GLYCOLYSIS_GLUCONEOGENESIS
KEGG_GLUTATHIONE_METABOLISM
KEGG_FATTY_ACID_METABOLISM
KEGG_CITRATE_CYCLE_TCA_CYCLE
KEGG_BUTANOATE_METABOLISM
KEGG_BETA_ALANINE_METABOLISM
KEGG_ASCORBATE_AND_ALDARATE_METABOLISM
KEGG_ALANINE_ASPARTATE_AND_GLUTAMATE_METABOLISM
Healthy
Liver Fibrosis
phenotype
-log10(p.adjust)
setSize
NES
C
Overview of Enriched Metabolite Sets (Top 25)
Galactose metabolism
Caffeine metabolism
Primary bile acid biosynthesis
Nicotinate and nicotinamide metabolism
Arginine and proline metabolism
Glyoxylate and dicarboxylate metabolism
Vitamin B6 metabolism
Steroid hormone biosynthesis
Sphingolipid metabolism
Ascorbate and aldarate metabolism
Citrate cycle (TCA cycle)
Valine, leucine and isoleucine degradation
Valine, leucine and isoleucine biosynthesis
Pantothenate and CoA biosynthesis
Histidine metabolism
beta-Alanine metabolism
Glycine, serine and threonine metabolism
Cysteine and methionine metabolism
D-Amino acid metabolism
Alanine, aspartate and glutamate metabolism
Arachidonic acid metabolism
Tryptophan metabolism
Arginine biosynthesis
Glutathione metabolism
Glycerolipid metabolism
-log10 (p-value)
P-value
0.6
0.4
0.2
0.0
Enrichment Ratio
2.5
5.0
7.5
10.0
D
Overview of Enriched Metabolite Sets (Top 25)
Primary bile acid biosynthesis
Caffeine metabolism
Ascorbate and aldarate metabolism
Alanine, aspartate and glutamate metabolism
Glyoxylate and dicarboxylate metabolism
Citrate cycle (TCA cycle)
Vitamin B6 metabolism
Valine, leucine and isoleucine degradation
Valine, leucine and isoleucine biosynthesis
Pantothenate and CoA biosynthesis
Nicotinate and nicotinamide metabolism
Galactose metabolism
Amino sugar and nucleotide sugar metabolism
Propanoate metabolism
Butanoate metabolism
Lysine degradation
Steroid hormone biosynthesis
Glycerolipid metabolism
Glycerophospholipid metabolism
Tryptophan metabolism
Biosynthesis of unsaturated fatty acids
Glutathione metabolism
Tyrosine metabolism
Histidine metabolism
beta-Alanine metabolism
-log10 (p-value)
P-value
0.4
0.3
0.2
0.1
0.0
Enrichment Ratio
2.5
5.0
7.5
10.0
12.5

781 **Figure 3**

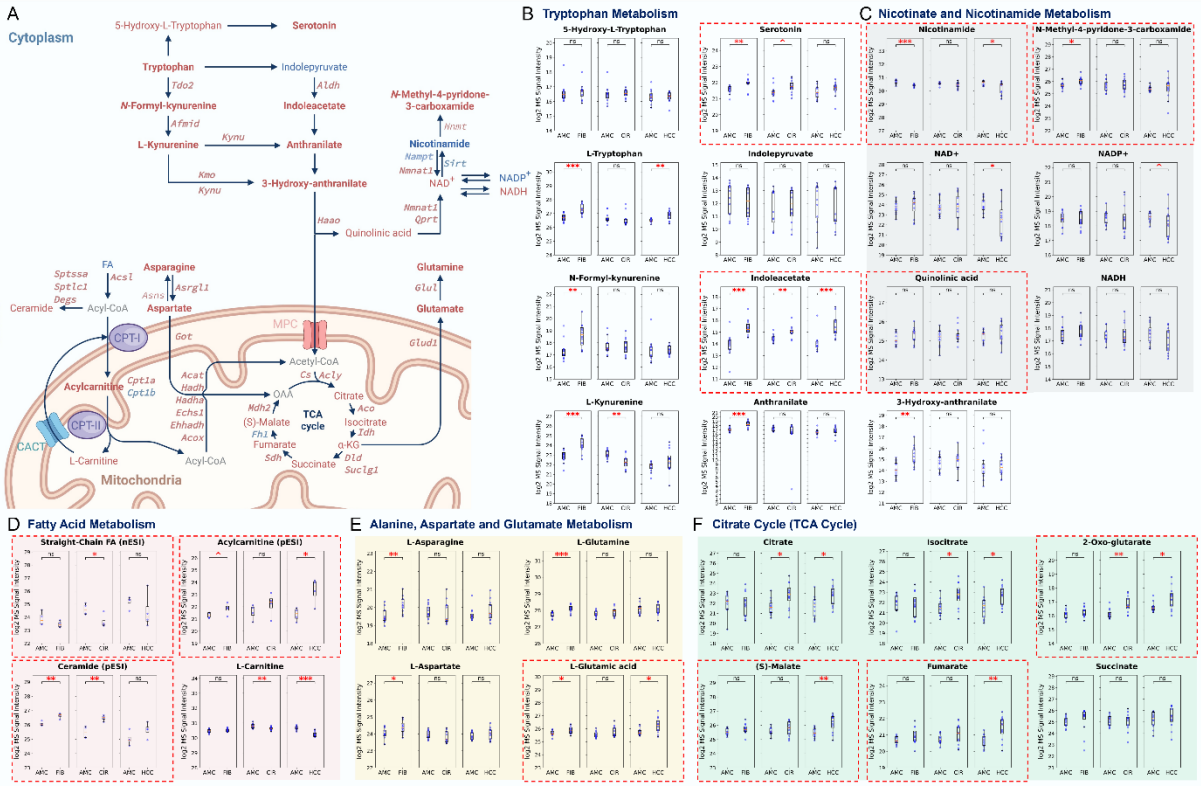

782

783 **Figure 4**

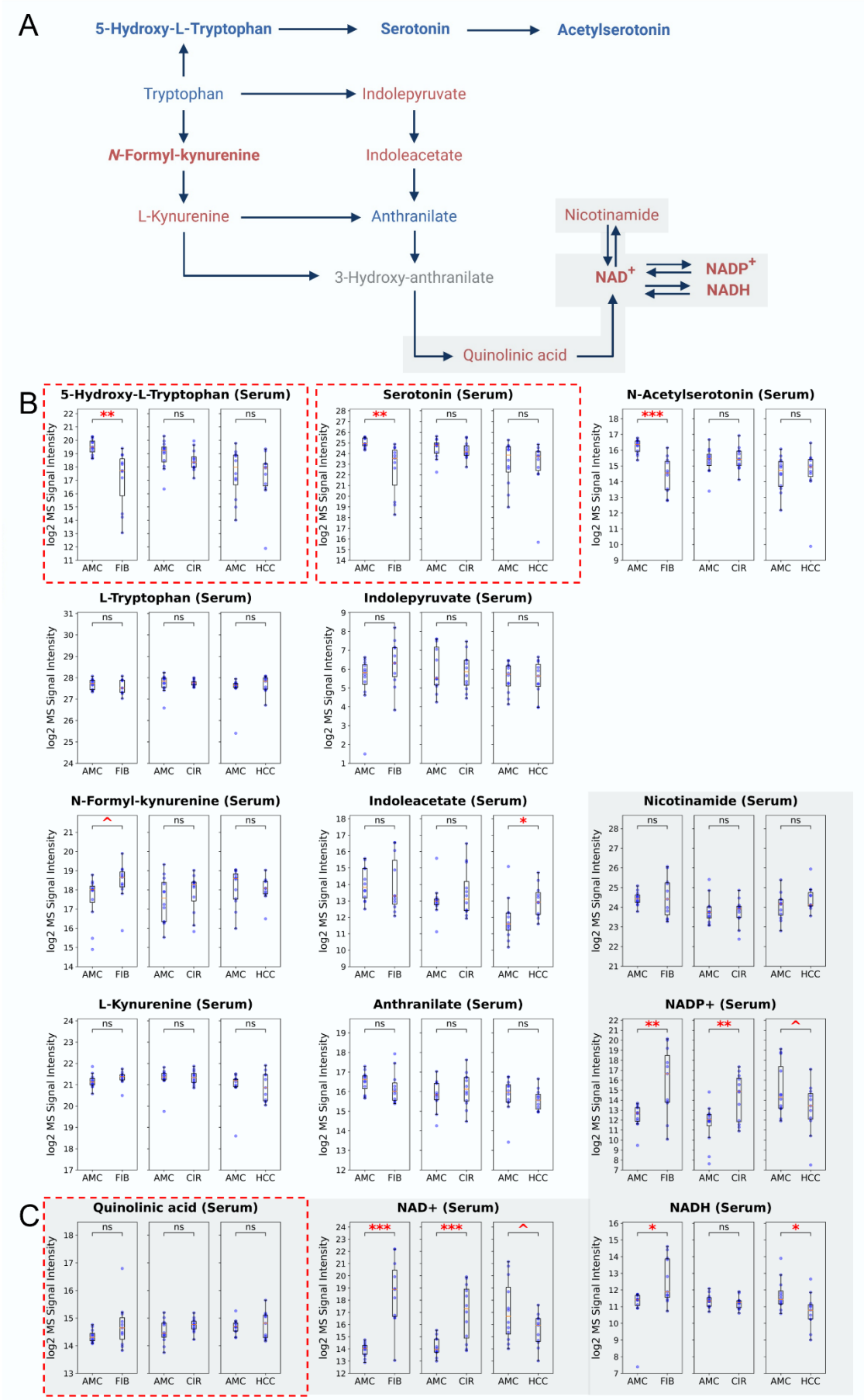

784

Figure 5

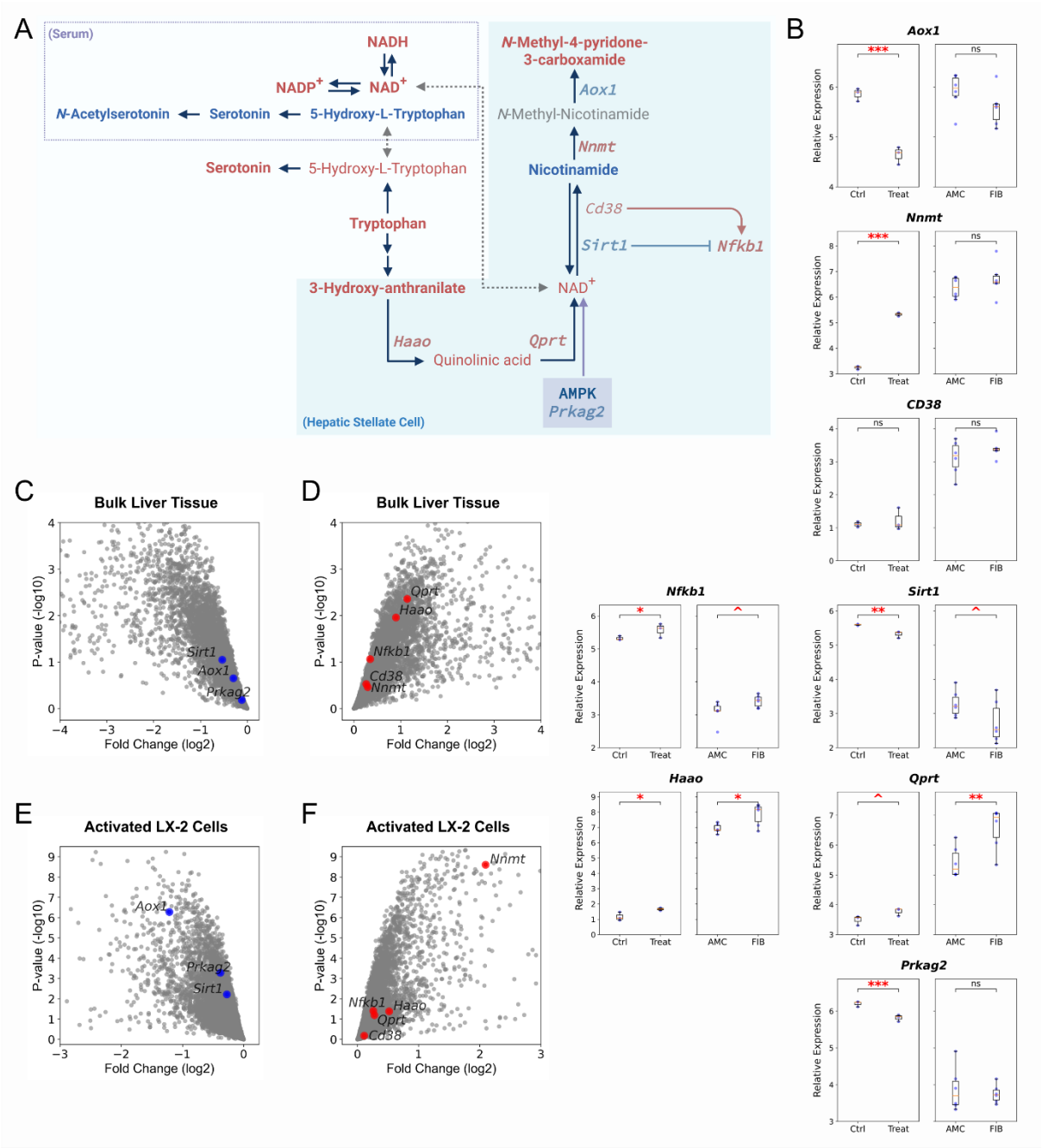
A
(Serum)
NADH
NADP+
NAD+
N-Acetylserotonin
Serotonin
5-Hydroxy-L-Tryptophan
Serotonin
5-Hydroxy-L-Tryptophan
Tryptophan
3-Hydroxy-anthranilate
Haao
Quinolinic acid
Qprt
N-Methyl-4-pyridone-3-carboxamide
Aox1
N-Methyl-Nicotinamide
Nnmt
Nicotinamide
Cd38
Sirt1
Nfkb1
NAD+
AMPK
Prkag2
(Hepatic Stellate Cell)
B
Aox1
Nnmt
CD38
Nfkb1
Sirt1
Haao
Qprt
Prkag2
Relative Expression
Ctrl
Treat
AMC
FIB
ns
C
Bulk Liver Tissue
P-value (-log10)
Fold Change (log2)
Sirt1
Aox1
Prkag2
D
Bulk Liver Tissue
Qprt
Haao
Nfkb1
Cd38
Nnmt
E
Activated LX-2 Cells
Aox1
Prkag2
Sirt1
F
Activated LX-2 Cells
Nnmt
Nfkb1
Haao
Qprt
Cd38

Figure 6

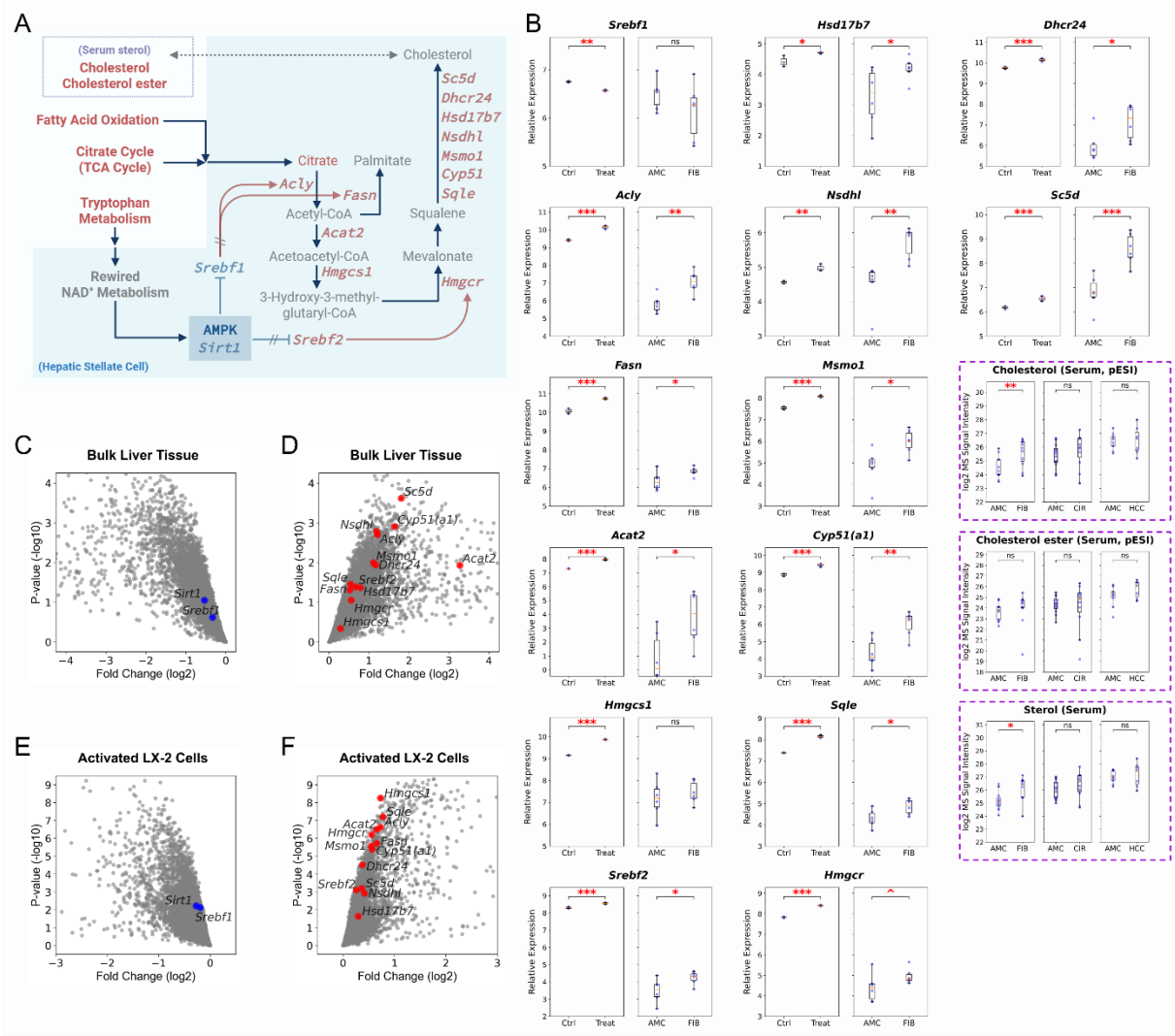
A
(Serum sterol)
Cholesterol
Cholesterol ester
Cholesterol
Fatty Acid Oxidation
Citrate Cycle
(TCA Cycle)
Citrate
Palmitate
Tryptophan
Metabolism
Acly
Fasn
Acetyl-CoA
Acat2
Squalene
Sc5d
Dhcr24
Hsd17b7
Nsdhl
Msmo1
Cyp51
Sqle
Rewired
NAD+ Metabolism
Srebf1
Acetoacetyl-CoA
Hmgcs1
Mevalonate
Hmgcr
3-Hydroxy-3-methyl-
glutaryl-CoA
AMPK
Sirt1
Srebf2
(Hepatic Stellate Cell)
B
Srebf1
Hsd17b7
Dhcr24
Acly
Nsdhl
Sc5d
Fasn
Msmo1
Acat2
Cyp51(a1)
Hmgcs1
Sqle
Srebf2
Hmgcr
Cholesterol (Serum, pESI)
Cholesterol ester (Serum, pESI)
Sterol (Serum)
Relative Expression
log2 MS Signal Intensity
Ctrl
Treat
AMC
FIB
CIR
HCC
C
Bulk Liver Tissue
P-value (-log10)
Fold Change (log2)
Sirt1
Srebf1
D
Bulk Liver Tissue
Sc5d
Nsdhl
Cyp51(a1)
Acly
Msmo1
Dhcr24
Acat2
Sqle
Srebf2
Fasn
Hsd17b7
Hmgcr
Hmgcs1
E
Activated LX-2 Cells
F
Activated LX-2 Cells